



Detection of soil physical properties of reclaimed land in open-pit mining area: feasibility of application of ground penetrating radar

Gubai Luo · Yingui Cao · Hanxiao Xu ·
Geng Yang · Shufei Wang ·
Yuhan Huang · Zhongke Bai

Received: 19 March 2020 / Accepted: 26 May 2021 / Published online: 8 June 2021
© The Author(s), under exclusive licence to Springer Nature Switzerland AG 2021

Abstract In order to obtain the typical soil physical properties of reclaimed land more quickly and accurately, the South Dump of the China Coal's Antaibao Open-Pit Mine in Pingshuo was focussed on in this paper, and ground penetrating radar (GPR) technology was utilized to detect the soil physical properties of reclaimed land in the mining area. The soil profile sampling and GPR detection methods were used to acquire the data. The gravel content of surface soil was analyzed by counting the number of isolated gravel signals in GPR images. The change of effective soil thickness was analyzed by establishing the fitting relationship between calibration depth and GPR image depth. The Topp's model was validated by comparing its inversion with the measured soil volumetric water content. And the Topp's model was further validated by the soil volumetric water content obtained from the Topp's model and which obtained from the wave velocity inversion. The results are as follows: (1) Based on the number of isolated gravel signals in GPR images, we could qualitatively analyze the gravel content of surface soil reclaimed in the mining area.

As the number of isolated gravel signals was greater, the gravel content of the surface soil was higher. (2) Using the known relative permittivity, electromagnetic wave velocity, and soil volumetric water content, the calibration depth and the reflection depth of the target (calibrator) of the GPR images were segmented, and the correlation between them is high. The fitting relationship (R^2) of each segment was higher than 0.940, and the average value of the five-segment R^2 was 0.966, which indicated more accurate detection of the effective soil thickness of the reclaimed land in the mining area. (3) GPR could be used to detect the soil volumetric water content of reclaimed land in mining area, and Topp's model was used for calculation of soil volumetric water content. The average deviation rate between the values from Topp's model and the measured values was 12%, and the average absolute value of the difference was 2%. In summary, the benefits of using GPR to detect soil physical properties of reclaimed land in mining area are as follows: (1) GPR can be used to detect soil layer thickness and surface gravel content faster and more accurately. (2) Topp model can also be used to calculate the soil moisture content of non-natural deposits such as reclaimed land in mining area.

G. Luo · Y. Cao (✉) · H. Xu · G. Yang · S. Wang ·
Y. Huang · Z. Bai
School of Land Science and Technology, China University
of Geosciences, Beijing 100083, China
e-mail: caoyingui@cugb.edu.cn

Y. Cao · Z. Bai
Key Laboratory of Land Consolidation and Rehabilitation,
Ministry of Natural Resources, Beijing 100035, China

Keywords Soil reconstruction · Ground penetrating radar (GPR) · Relative permittivity · Soil layering · Gravel content · Soil volumetric water content

China is the largest producer of coal in the world. By the end of 2017, China reported the construction of 4980 coal mines with a total production capacity of 4.36 billion tons (Li, 2018). At the same time, coal mining has also caused numerous environmental problems, such as landslides, collapses, debris flow, ground subsidence and other geological disasters, land destruction, and water pollution caused by wastewater and waste residue (Cao et al., 2017; Ma et al., 2012). In addition, coal mining can lead to land use conflicts and the loss of biodiversity and habitat (Cao et al., 2018). Land reclamation refers to the activities in which the land damaged by production or construction activities or natural disasters becomes available through land remediation technology (Wang, 2011). Reclamation and rehabilitation on damaged land in mining area can improve the ecological environment and prevent land use conflicts of the mining area. The promulgation of the *Land Reclamation Regulations* (2011), the *Completion Standards on Land Reclamation Quality* (2013), and related technical regulations for land reclamation has ensured that land reclamation have been regulated and standardized, and further highlight the importance of land reclamation.

Soil reconstruction was the core content of land reclamation, and the quality of reconstructed soil was the main criterion to test the effect of soil reconstruction (Hu et al., 2005a, b). Through the process of soil reconstruction, the soil physical properties, including thickness of the soil layers, gravel content of surface soil, and water content, were altered, which influenced the effectiveness of the vegetation restoration in mining area (Guo et al., 2015; Li et al., 2007; Ye et al., 2008). The relationship between soil thickness and vegetation growth was well documented (Li et al., 2016). Optimal soil layer thickness was beneficial to vegetation growth, microbial activity, and the improvement of soil fertility (Chen et al., 2016; Meerveld & McDonnell, 2006). Soil gravel content primarily affected soil temperature and moisture (Cerd, 2001). Topsoil-covered gravel could reduce the rill flow rate and erosion rate (Wang et al., 2011). In addition, the soil gravel influenced the content of various elements, such as soil carbon and nitrogen, and the solute transport process (Certini et al., 2004). Soil water content directly affected vegetation growth and plant diversity (Ersahin & Brohi, 2006; Guo et al., 2005; Huang et al., 2004). In the process of land reclamation in mining area, it was necessary to

improve the water storage capacity of the soil, which provided the necessary conditions for the restoration of vegetation (Yu et al., 2016). Therefore, it is of practical significance to study the soil physical properties of reclaimed land, such as soil thickness, gravel content, and soil volumetric water content.

As a shallow geophysical detection technology, GPR has the characteristics of fast, convenient, non-destructive, continuous, repeatable detection, and large area measurement. The application of GPR in soil detection at home and abroad had gradually expanded (Hubbard et al., 2002; Hu et al., 2005a, b; Lei & Bian, 2008; Wang et al., 2013; Ratto et al., 2014). There were few examples of the application of the GPR technology in the detection of soil gravel content, and to date, evaluation and prediction had been limited to experimental analysis, but the potential for wider application of the technology was evident (Carl & Peter, 1996; He et al., 2009). Zenone et al. (2008) showed that the resolution of GPR increased with an increase in antenna frequency. The higher the frequency, the finer the detection capability. These studies indicated that high-frequency GPR could be utilized to detect surface soil gravel content (Zenone et al., 2008). Yang et al. (2014) believed that it was feasible to use GPR tomography technology for the exploration of complex geological structures in mining area. Yu et al. (2011) used GPR technology to detect the thickness of the gravel layer, and the results were in good agreement with the thickness of the soil obtained using traditional investigation methods, with marginal errors. Benedetto et al. (2010) showed that GPR images had the potential to accurately determine soil volumetric water content. Wu et al. (2014) detected soil volumetric water content in loam and sandy soil using GPR and pointed out that the accuracy of GPR in the detection of soil volumetric water content was higher than that of time domain reflectance technology (TDR). However, there were few studies on the quantitative determination of effective soil thickness and soil gravel content in reclaimed coal mine area by using GPR. GPR had been used to detect soil volumetric water content, but there were few studies on the detection of soil volumetric water content in reclaimed mining area.

Different soil physical properties have different signal characteristics in GPR images. Soil effective thickness is shown as a continuous low-frequency signal in GPR images; soil gravel is shown as an

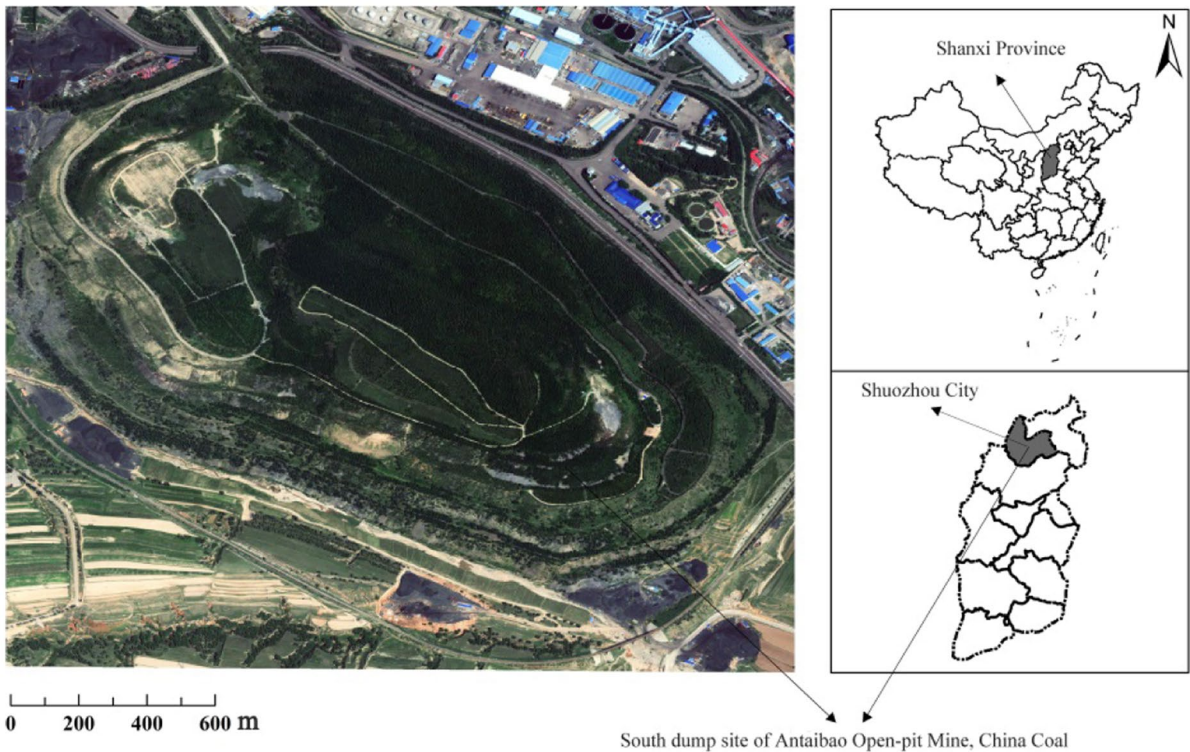


Fig. 1 South Dump site of China Coal Antaibao Open-Pit Mine

open-down parabolic in GPR images, and soil volumetric water content difference is shown as a strong and weak change of amplitude signal in GPR images.

Therefore, this study focussed on the soil physical properties of China Coal Antaibao Coal Mine South Dump in Pingshuo, explored the methodology and effectiveness of GPR in detecting the physical properties of reconstruct soil, provided support for detecting physical properties of reconstruct soil by GPR, and could be used to guide land remediation.

Materials and methods

Study area survey

The study area is located in Pinglu District, Shuozhou City, Shanxi Province (Fig. 1), and the study area (the South Dump) is an early outer dump of the China Coal Antaibao Open-Pit Mine, Pingshuo City. The Antaibao Mine is located at 112° 11'–113° 30' east and 39° 23'–39° 37' north, where it is with a temperate

semi-arid continental climate, and characterized by strong winds in winter and spring. The annual average temperature is 4.8–7.8 °C; the annual precipitation is about 450 mm, and the annual evaporation is approximately 5 times the annual precipitation. The

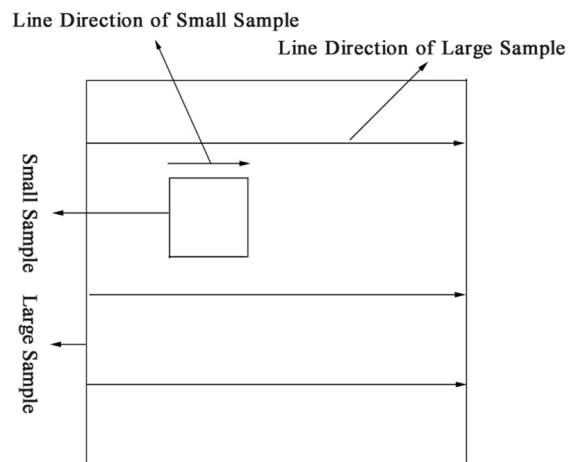


Fig. 2 Quadrat layout and line graph

altitude of the dumping site is 1360–1465 m, and the slope of which is 20–40°. The South Dump is a mixed earth-rock dump, in which 46.98% of the rocks are greater than or equal to 50 mm.

Sample and profile creation

Twenty-three large squares of 10 m×10 m in size were set up at the South Dump site, and three 10-m-long measuring lines were set up in the squares (Fig. 2). A smaller square of 1 m×1 m was established in the middle of the larger square, numbered S₁–S₂₃. Within the smaller squares, a soil profile with length×width×depth of 1.2 m×1 m×1 m was excavated and numbered P₁–P₂₃, which was used to obtain soil samples and calibrate the depth of detection. The sampling time was from May 2018 and August 2018.

GPR detection and parameter determination

GPR detection principle

GPR is a non-destructive detection technology that uses the reflection of electromagnetic waves to detect underground media (Fig. 3). The GPR is composed of a main frame and an aerial. When the electromagnetic wave emitted by transmitting aerial encounters a medium with different relative permittivity in the process of propagation, the electromagnetic wave will be emitted at the interface of the two media, which makes the amplitude and waveform of the electromagnetic wave change accordingly. According to the received radar waveform, intensity, and two-way travel time, the shape,

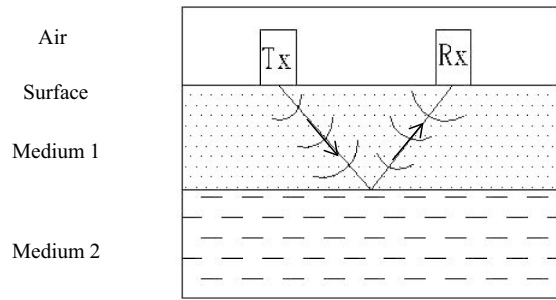
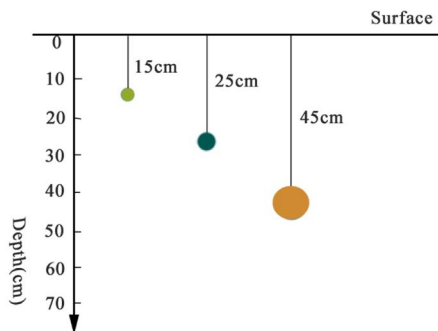


Fig. 3 GPR working principle

spatial position, and structure of the underground target can be interpreted (Liang, 2012; Neal, 2004).

GPR detection process The electrical properties of a steel pipe and the surrounding soil medium are distinct. So, in this test, the detection depth was calibrated using steel pipes. After the soil profile was excavated, steel pipes with diameters of 3 cm, 5 cm, and 9 cm were drilled into the soil profiles at various depths (Fig. 4), and then GPR with a 900-MHz aerial was used to detect the surface land (Fig. 2). The equipment used in this test was the latest Ltd-2600 GPR provided by the 22nd Research Institute of the China Electronic Science and Technology Group Corporation. The detection speed was 0.10 m/ns; the relative permittivity was 8 (8 is the empirical value of the dielectric constant of sand); the time window was 25 ns; the number of sampling point was 512, and the distance between channels was 0.20 cm.

Fig. 4 Steel pipes’ depth calibration. The depth of the steel pipe is 15 cm, 25 cm, and 45 cm



Method of parameter determination

The propagation velocity of the electromagnetic wave in the medium is determined by the true depth of the medium and the propagation time of the electromagnetic wave in the medium. The calculation formula of the wave speed is shown in Eq. (1)

$$v = 2 \times d/t \tag{1}$$

where v is the propagation velocity of electromagnetic waves in the soil, in which unit is m/ns; d is the calibration depth of the steel pipe, refers to the true burial depth of the calibrator in soil, in which unit is m, and t is the two-way travel time of electromagnetic waves in the soil, in which unit is ns.

The relative permittivity is the ability of a substance to hold a charge, in which size determines the ability of the medium to absorb or reflect electromagnetic waves. The calculation of the relative permittivity is shown in Eq. (2)

$$\epsilon = (c/v)^2 \tag{2}$$

where ϵ is the relative permittivity, which is the ratio of permittivity to absolute permittivity in vacuum; c is the speed of light with the value of 3.00×10^8 m/s; v is the speed at which the electromagnetic wave propagates in the medium, and which is the ratio of the depth of the soil layer to the propagation time of the electromagnetic wave in this paper.

The soil volumetric water content is the amount of water contained in the soil. Previous studies have determined the empirical formula for using GPR to detect soil volumetric water content, and the Topp’s model is the most commonly used model at present. The empirical formula for inversion of soil volumetric water content using Topp’s model is shown in Eq. (3) (Topp et al., 1980)

$$\theta = (4.3\epsilon^3 \times 10^{-6} - 5.5\epsilon^2 \times 10^{-4} + 2.92\epsilon \times 10^{-2} - 5.3 \times 10^{-2})/100 \tag{3}$$

where θ is the soil volumetric water content and ϵ is the relative permittivity.

Collection and testing of soil samples

Soil ringknife samples were collected every 10 cm in the profile and weighed immediately. The dry weight

and the weight of soil water were obtained by drying method, and the soil volumetric water content of soil was calculated by Eq. (4). The equation is as follows:

$$\theta_v = \frac{m_{wet} - m_{dry}}{v} \tag{4}$$

where θ_v is soil volumetric water content, m_{wet} is soil wet weight, in which unit is g, m_{dry} is soil dry weight, in which unit is g; v is ringknife volume, in which size is 100 cm^3 , and water density is 1 g/cm^3 .

Results and analysis

Parameter determination

The parameters were determined by the steel pipe calibration or layered calibration, as shown in Fig. 5. The average propagation velocity of electromagnetic waves to the calibrator (target) was obtained using

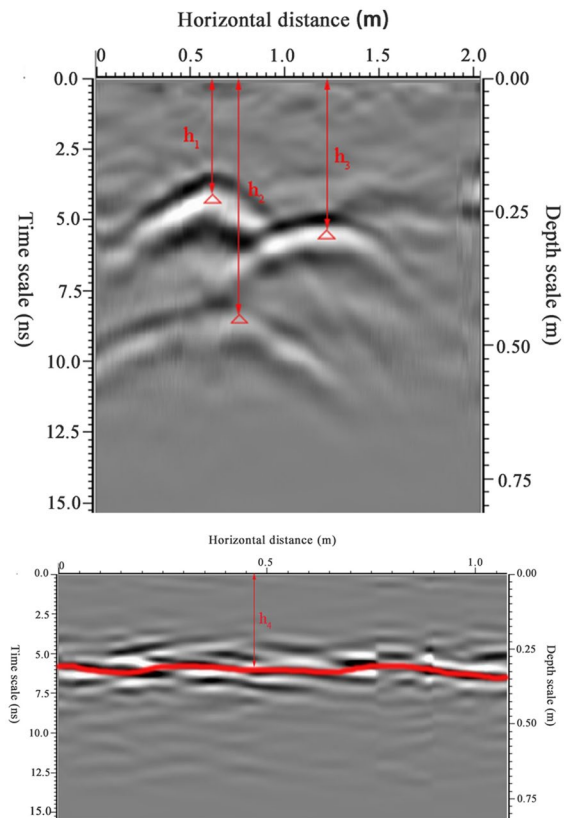


Fig. 5 Depth calibration of each profile based on GPR images

Table 1 Relevant parameters at calibration depths

Profile	Calibration type	GPR images depth (cm)	True depth (cm)	Two-way travel time (ns)	Electromagnetic wave velocity (m/ns)	Relative permittivity	
S1	Steel pipe	14.0	19	2.40	0.1583	3.59	
		19.0	24	4.60	0.1043	8.27	
		33.0	43	7.00	0.1229	5.96	
S2	Layering	26.0	25	5.26	0.0951	9.96	
		26.0	26	5.07	0.1026	8.56	
		54.0	51	10.33	0.0987	9.23	
S3	Steel pipe	10.0	13	1.38	0.1884	2.54	
		15.0	17	2.47	0.1377	4.75	
		25.0	30	3.85	0.1558	3.71	
S4	Steel pipe	19.0	20	3.60	0.1111	7.29	
		12.0	13	2.30	0.1130	7.04	
		31.0	33	5.90	0.1119	7.19	
S5	Steel pipe	23.0	23	4.37	0.1053	8.12	
		15.0	12	2.95	0.0814	13.60	
		38.0	35	7.32	0.0956	9.84	
S6	Steel pipe	15.4	15	2.97	0.1010	8.82	
		10.3	10	1.92	0.1042	8.29	
		25.7	25	4.89	0.1022	8.61	
S7	Steel pipe	19.5	17	3.68	0.0924	10.54	
		15.0	10	2.44	0.0820	13.40	
		34.5	27	6.12	0.0882	11.56	
S8	Steel pipe	42.0	45	7.71	0.1167	6.60	
		19.8	15	3.74	0.0802	13.99	
		14.4	11	2.73	0.0806	13.86	
S9	Steel pipe	34.2	26	6.47	0.0804	13.93	
		11.0	10	2.10	0.0952	9.92	
		18.9	14	3.30	0.0848	12.50	
S10	Steel pipe	29.9	24	5.40	0.0889	11.39	
		16.6	16	3.37	0.0950	9.98	
		46.5	40	8.77	0.0912	10.82	
S11	Steel pipe	11.0	13	2.70	0.0963	9.71	
		6.0	9	2.00	0.0900	11.11	
		17.0	22	4.70	0.0936	10.27	
		19.0	16	3.49	0.0917	10.71	
		42.5	40	8.19	0.0977	9.43	
S12	Steel pipe	16.4	14	3.09	0.0906	10.96	
		13.1	12	2.39	0.1004	8.93	
		29.5	26	5.40	0.0963	9.71	
		11.6	12	2.23	0.1076	7.77	
		41.1	38	7.79	0.0976	9.46	
S12	Steel pipe	0–15	18.5	15	3.48	0.0862	12.11
		15–27	12.0	12	3.37	0.0712	17.75
		0–26	37.2	26	6.75	0.0800	14.06
		26–37	10.2	11	2.75	0.0800	14.06
		0–37	49.4	37	9.50	0.0779	14.83

Table 1 (continued)

Profile	Calibration type	GPR images depth (cm)	True depth (cm)	Two-way travel time (ns)	Electromagnetic wave velocity (m/ns)	Relative permittivity	
S13	Steel pipe	0–11	12.2	11	2.31	0.0952	9.92
		11–25	16.9	14	3.17	0.0883	11.54
S14	Steel pipe	0–25	29.1	25	5.48	0.0912	10.81
		0–13	15.6	13	2.94	0.0884	11.51
		13–24	13.9	11	2.62	0.0840	12.76
S15	Layering steel pipe	0–24	29.5	24	5.56	0.0863	12.08
		0–14	11.0	14	3.01	0.0930	10.40
		14–26.5	18.0	12.5	3.37	0.0742	16.35
S16	Steel pipe	0–26.5	29.0	26.5	6.38	0.0831	13.04
		0–13	14.9	13	2.90	0.0897	11.20
		13–25	14.4	12	2.62	0.0916	10.73
S17	Steel pipe	0–25	29.3	25	5.52	0.0906	10.97
		25–41	16.6	15	3.13	0.0958	9.80
		0–41	45.9	41	8.65	0.0948	10.01
		0–20	20.8	20	3.88	0.1031	8.47
		20–29	8.50	9	1.54	0.1169	6.59
S18	Steel pipe	0–29	29.3	29	5.42	0.1070	7.86
		29–49	16.9	20	3.41	0.1173	6.54
		0–49	45.9	49	8.75	0.1120	7.17
		0–18	18.7	18	3.57	0.1008	8.85
		18–28	11.6	10	1.99	0.1005	8.91
S19	Steel pipe	0–28	30.3	28	5.61	0.0998	9.03
		0–17	18.4	17	3.56	0.0955	9.87
		17–27	11.9	10	2.16	0.0926	10.50
S20	Steel pipe	0–27	30.3	27	5.71	0.0946	10.06
		0–15	15.4	15	2.97	0.1010	8.82
		15–26	13.2	11	2.31	0.0952	9.92
S21	Layering steel pipe	0–26	28.5	26	5.28	0.0985	9.28
		0–15	23.2	15	4.18	0.0718	17.47
		15–27	14.8	12	3.08	0.0779	14.82
S22	Steel pipe	0–27	38.0	27	7.26	0.0744	16.27
S23	Steel pipe	0–15	21.8	15	4.11	0.0730	16.89
		0–15	16.6	15	3.13	0.0958	9.80
		15–30	13.5	15	2.55	0.1176	6.50
		0–30	30.1	30	5.68	0.1056	8.07
		20–47	19.0	17	3.57	0.0952	9.92
		0–47	49.1	47	9.25	0.1016	8.72

the calibration depth (Fig. 5), and the corresponding timescale of the target (steel pipe and layered interface) on the GPR images was obtained using Eq. (1). The average relative permittivity of the calibrator to

the surface land was obtained by using Eq. (2). The two-way travel time of electromagnetic wave propagation to the calibration object was read from the GPR images (Table 1).

Gravel content

The signal of the isolated gravel on the GPR images gave a downward parabola, as shown in the red circle of Fig. 6. This paper evaluated the gravel content of soil by counting the number of isolated gravel signals in the surface soil in different sample GPR images of reclaimed land in mining area. The results were verified in the corresponding sample excavation section, as shown in Fig. 7. Based on the resolution of GPR, deeper gravel would not be detectable. Therefore, the isolated gravel signals with a depth of inside 30 cm in the GPR images of 10 samples (S_1 – S_{10}) were counted (Table 2). The corresponding profiles (P_1 – P_{10}) were excavated in each sample, and the gravel situation of each profile was recorded (Table 3). Comparing Tables 2 and 3, as a whole, the number of isolated gravel signals on the GPR images could correspond well with the debris of the profile, which indicated that GPR could be used to detect the gravel content of the surface soil in the reclaimed land. In addition, P_1 , P_3 , P_5 , P_7 , and P_8 were pure soil profiles, but there were also a certain number of isolated gravel signals in their corresponding ground penetrating radar images. This was because the GPR was moving during the detection. It also indicated that in addition to the

existence of potentially isolated gravel in the soil, there may be isolated heterogeneous bodies with differences in the relative permittivity of the soil. The profile of P_9 was composed of soil and rock, and there were many isolated gravels, but the number of isolated gravel signals in corresponding GPR images was relatively small, which indicated that some gravel could not be detected by GPR in soil, which was related to the aerial used in GPR detection and the burial depth of isolated gravel in soil. The higher the frequency of the aerial, the smaller the diameter of the isolated body could be detected, and the larger the buried gravel in the soil, the less likely it was detected by the GPR.

Effective soil thickness

Soil profile was made up of overlapped layers with different morphological characteristics, and these levels were roughly horizontal, called soil occurrence layers or soil layers. The soil thickness that plants could grow was the effective soil thickness. The penetration depth of the electromagnetic wave in the medium was related not only to the aerial frequency but also to the relative permittivity of the medium. In this paper, a relationship between the calibration depth of the object and the depth of GPR images was established, based

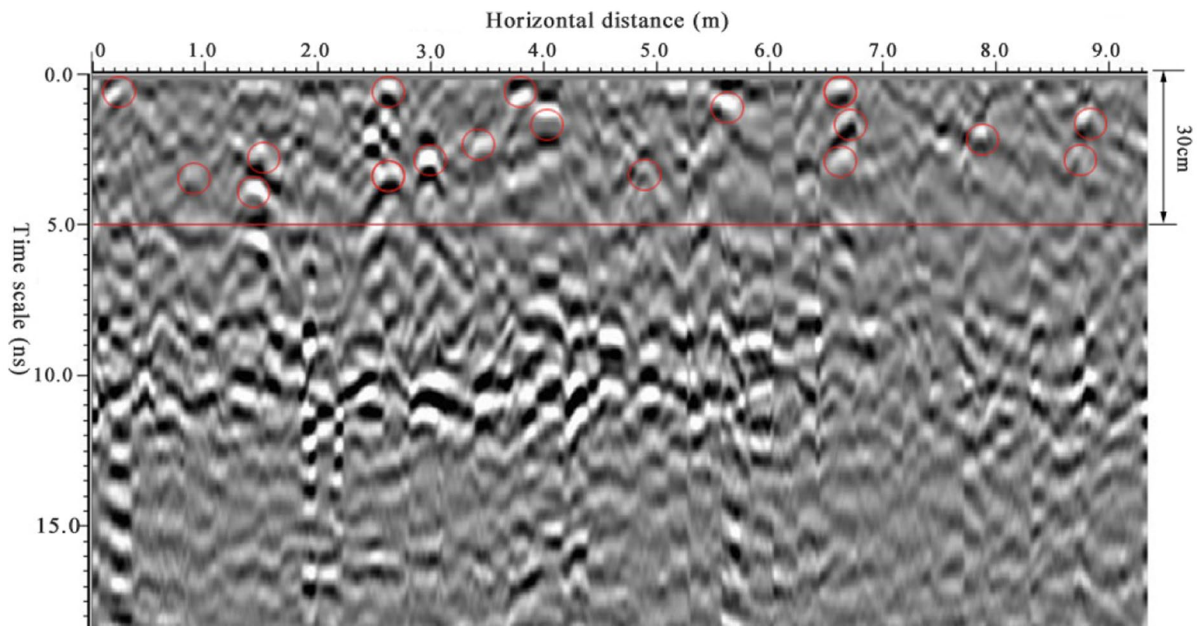


Fig. 6 Isolated gravel signal in GPR images (profile P_2)



Fig. 7 Profile method to verify the gravel content of the sample (profile P₄)

on the propagation speed of the electromagnetic wave in the medium, relative permittivity, and soil volumetric water content. After setting the time window and electromagnetic wave velocity, the burial depth of the target was directly determined by the depth of the signal map. The linear relationship between the calibration depth of the target and the depth of GPR images was established, $R^2=0.890$, as shown in Fig. 8a, without considering the difference of relative permittivity, electromagnetic wave velocity, and soil volumetric water content. According to the difference of relative permittivity, electromagnetic wave velocity, and soil volumetric water content, a linear relationship between the calibration depth of the target and the depth of the GPR images was established. The linear relationship could be divided into five sections (formula 5). The fitting images of each linear relationship are shown in b–f of Fig. 8. From the graph, R^2 of each segment was greater than 0.940, and the average value of R^2 of the five segments was 0.966. The correlation was very high. It was

found that the correlation between the calibration depth of the target and the depth of the GPR images was higher after segmentation according to relative permittivity, electromagnetic wave velocity, and soil volumetric water content.

$$f(x) = \begin{cases} 0.75x(0.07 < v \leq 0.08 \text{ or } 14 < \epsilon \leq 18 \text{ or } 26 < \theta \leq 32) \\ 0.80x(0.08 < v \leq 0.09 \text{ or } 11 < \epsilon \leq 14 \text{ or } 21 < \theta \leq 26) \\ 0.92x(0.09 < v \leq 0.10 \text{ or } 9 < \epsilon \leq 11 \text{ or } 17 < \theta \leq 21) \\ 0.99x(0.10 < v \leq 0.11 \text{ or } 7 < \epsilon \leq 9 \text{ or } 14 < \theta \leq 17) \\ 1.07x(0.11 < v \leq 0.12 \text{ or } 6 < \epsilon \leq 7 \text{ or } 11 < \theta \leq 14) \end{cases} \quad (5)$$

where v is the electromagnetic wave velocity in m/ns, ϵ is the relative permittivity, θ is the soil volumetric water content, x is the thickness of the soil layer read in the GPR images, and $f(x)$ is effective soil thickness.

During detection, the aerial frequency was set to 900 MHz, the time window was 25 ns, and the electromagnetic wave velocity was 0.1 m/ns.

The GPR images for the 9 profiles that were not included in the model construction were introduced into the fitting model of (5) for inversion. The inversion results are shown in Table 4. It could be seen from Table 4 that the absolute value of the difference between the calibration depth and the inversion depth was at most 2.49 cm and the minimum was 0.50 cm, and the maximum deviation between the calibration depth and the inversion depth was 1.04 cm, and the average deviation rate was 5.61%.

Soil volumetric water content

Topp’s model is the most widely used model to determine soil volumetric water content. The soil volumetric water content at each calibrated depth was obtained by Topp’s model (Eq. 3) from the relative permittivity of soil at each calibrated depth. From Table 5, the maximum value of the absolute difference value between the soil volumetric water content obtained by empirical formula and the measured value was 3.90%, the minimum was 0, and the average value was 2%. The maximum deviation rate of soil volumetric water content measured by the two methods was 25%; the minimum deviation rate was 0, and the average deviation rate was 12%.

Table 2 Statistics of isolated gravel signals of various GPR images

Sample	S1	S2	S3	S4	S5	S6	S7	S8	S9	S10
Number of isolated gravel signals	26	50	10	34	22	64	20	22	28	52

Table 3 Sample section gravel profile

Profile	P ₁	P ₂	P ₃	P ₄	P ₅
Profile condition	Pure soil profile	Earth and stone mixed, more isolated gravel	Pure soil profile	Earth and stone mixed, less gravel	Pure soil profile
Profile	P ₆	P ₇	P ₈	P ₉	P ₁₀
Profile condition	Mixed earth and rock, Isolated gravel is plentiful	Pure soil profile	Pure soil profile	Earth and stone mixed, less gravel	Earth and stone mixed, more isolated gravel

Wave velocity inversion of soil volumetric water content

The study area was located at the South Dump of the China Coal Antaibao Open-Pit Coal Mine, which had sandy soil and was a low conductivity medium. Therefore, the soil volumetric water content had the greatest influence on the propagation speed of electromagnetic waves in the soil. So, the change in soil volumetric water content could be determined by the propagation velocity of electromagnetic waves in the soil. In this paper, the relationship between the electromagnetic wave propagation velocity and the measured soil volumetric water content (Table 5) was established by the measured values at 47 calibration depths (Fig. 9).

From Fig. 9, the fitting relationship between the soil volumetric water content and the electromagnetic wave velocity exhibited a cubic function relationship; the R^2 value was 0.836, and the fitting effect was good. This showed the same relationship trend as Topp's model, and the regression order was 3. With an increase in electromagnetic wave velocity, the soil volumetric water content decreased gradually. When the electromagnetic wave velocity reached 0.16 m/ns, the curvature reached a minimum. Then, with a further increase in electromagnetic wave velocity, the soil volumetric water content did not decrease. However, Table 5 shows that when the velocity of electromagnetic wave was greater than 0.16 m/ns, the soil volumetric water content decreased significantly, which indicated that when the velocity of electromagnetic wave was greater than 0.16 m/ns, the fitting model of electromagnetic wave velocity and soil volumetric water content was no longer applicable.

The electromagnetic wave propagation velocity at each calibration depth was concentrated from 0.80 to 0.11 m/ns, and the soil volumetric water content was concentrated at 10–25%.

The 10 electromagnetic wave velocity values were substituted into the fitting relationship model in Fig. 9 to determine the soil volumetric water content, and the results are shown in Table 6. Table 6 shows that the maximum absolute value, the minimum absolute value, and the average absolute value of the difference between soil volumetric water content measured by gravimetric method and, respectively, inverted by wave velocity were 3.95%, 0.75%, and 2.90%. Maximum average deviation, minimum average deviation, and average deviation rate of the difference between soil volumetric water content measured by gravimetric method and inverted by wave velocity were 16%, 0.10%, and 12%.

The soil volumetric water content value obtained by Topp's model and the wave velocity inversion was compared. The average absolute value of the difference between the soil volumetric water content and the measured soil volumetric water content obtained by Topp's model was 2%, and the average value of the absolute pasc of the difference between the soil volumetric water content and the measured soil volumetric water content obtained by wave velocity inversion was 2.62%, and the difference between them was 0.62%. The average deviation rate of the measured values and the inversion values of the two methods was equal, both being 12%. This showed that the Topp's model was also applicable to the calculation of soil volumetric water content in reclaimed land in coal mining area.

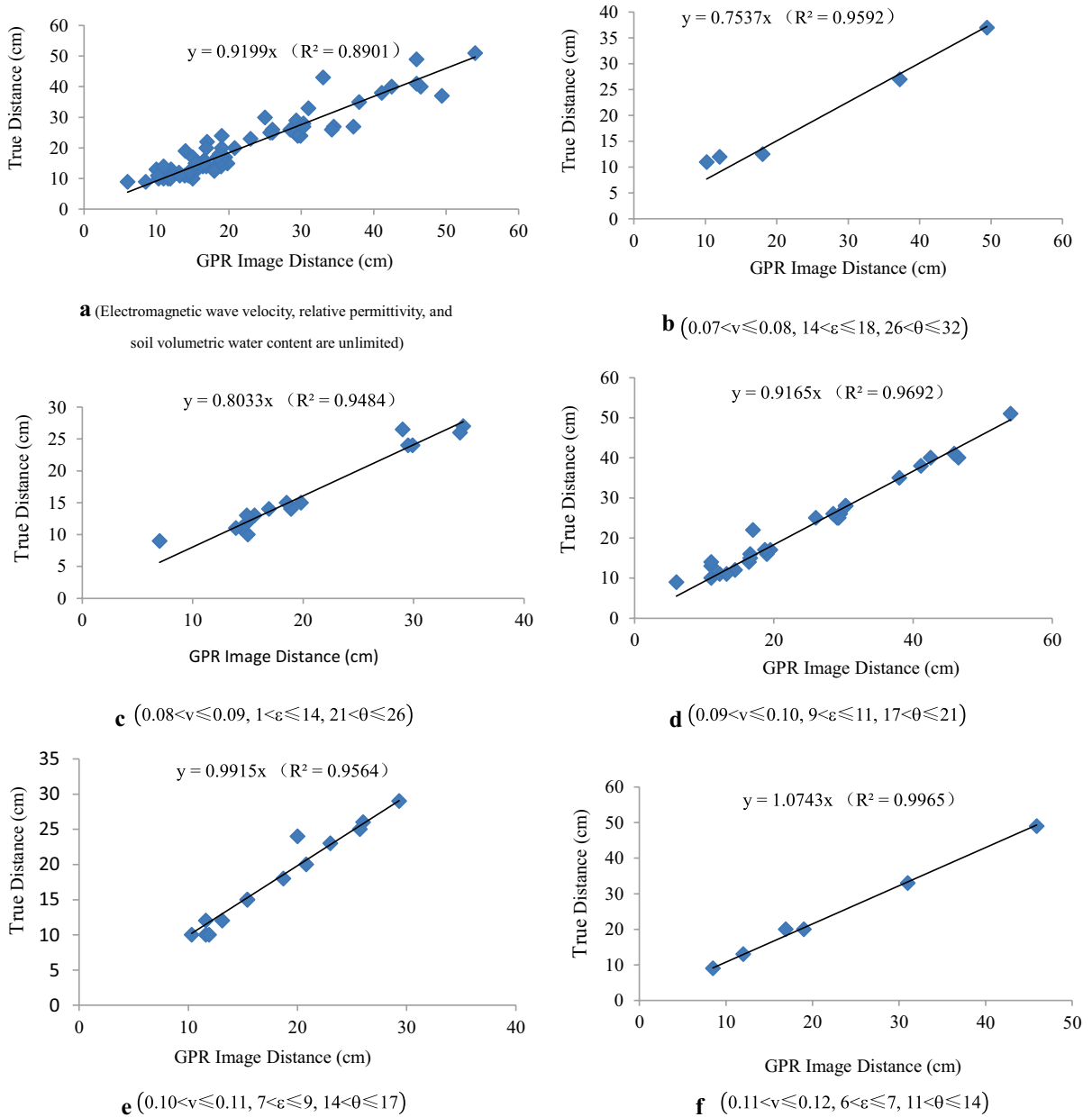
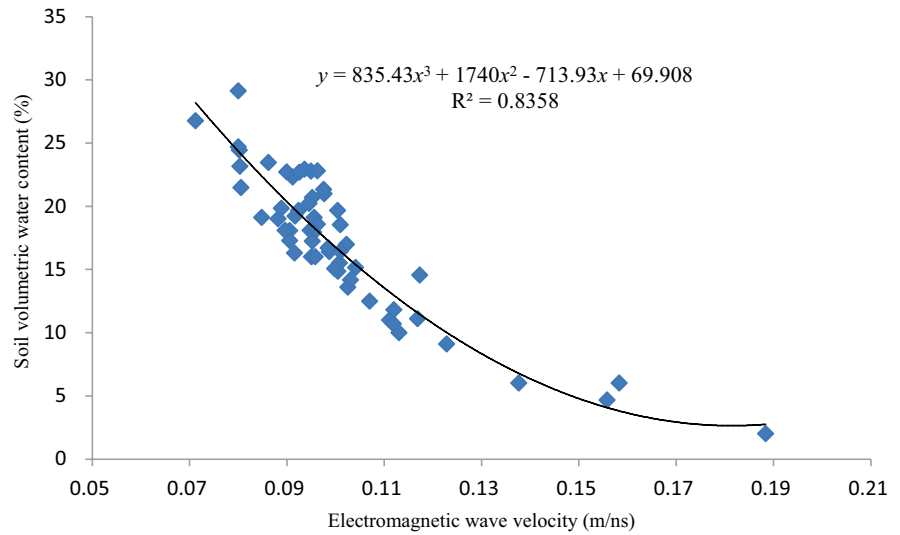


Fig. 8 The relationship between the reflectance depth of the calibrator and the true burial depth of the calibrator in GPR images of the calibrator in GPR images **a**: The linear relationship between the calibration depth of the target and the

depth of GPR images when the values of v , ε and θ are unlimited; **b-f**: The linear relationship between the calibration depth of the target and the depth of GPR images under different values of v , ε and

Fig. 9 Inverse relationship between soil volumetric water content and electromagnetic wave velocity



Discussions

Reconstructing soil gravel content

Through the number of isolated gravel signals in the GPR images, the gravel content of the surface soil in the reclaimed land of the mining area could be qualitatively analyzed. Isolated gravel and its surrounding soil were two different media with permittivity differences. Electromagnetic waves were reflected at the interface between the gravel and the soil, and appear as a parabolic signal feature of the opening down on the ground penetrating radar images (Qian et al., 2004), as shown by the red rectangle in Fig. 10. The GPR transmitting aerial emitted a spherical wave to the ground (Wang & Wu,

2010), so the signal from the isolated gravel in the images was a parabola with a downward opening. The greater the number of parabolas, the more isolated debris was present in the soil, and the higher the gravel content of the surface soil. Therefore, it was theoretically feasible to analyze the gravel content of the topsoil by counting the number of signals of isolated gravel. The higher the aerial frequency, the larger the resolution, and a greater range of sizes of gravel could be detected (Anchueta et al., 2016; Berton et al., 2019). Shakas and Linde (2017) showed that the heterogeneity of cracks could be detected by GPR according to the electrical conductivity differences of different media (Shakas & Linde, 2017). Yamase et al. (2018) showed that GPR could detect the distribution of vegetation roots

Table 4 Comparison of calibration depth and model inversion depth of each profile

Wave speed (m/ns)	Relative permittivity	Soil volumetric water content (%)	GPR images depth (cm)	Calibration depth (cm)	Inversion depth (cm)	Calibration-inversion (cm)	Calibration-inversion deviation rate (%)
0.072	17.47	0.312	23.2	15	17.49	-2.49	16.6
0.078	14.82	0.273	14.8	12	11.15	0.85	7.1
0.074	16.27	0.295	38	27	28.64	-1.64	6.1
0.073	16.89	0.304	21.8	15	16.43	-1.43	9.5
0.096	9.80	0.184	16.6	15	15.21	-0.21	1.4
0.118	6.50	0.115	13.5	15	14.50	0.50	3.3
0.106	8.07	0.149	30.1	30	29.84	0.16	0.5
0.095	9.92	0.187	19	17	17.41	-0.41	2.4
0.102	8.72	0.163	49.1	47	48.68	-1.68	3.6

Table 5 Comparison of soil volume moisture content measured by gravimetric method and inverted by Topp's model

Calibration depth (cm)	19.0	43.0	25.0	26.0	51.0	13.0	17.0	30.0	20.0	13.0	33.0	35.0	15.0	10.0	16.0	9.0	29.0	20.0	49.0
Wave speed (m/ns)	0.16	0.12	0.10	0.10	0.10	0.19	0.14	0.16	0.11	0.11	0.11	0.10	0.10	0.10	0.09	0.12	0.11	0.12	0.11
Inversion of soil volumetric water content by Topp's model (%)	4.00	10.00	19.00	16.00	17.00	2.00	7.00	5.00	13.00	13.00	13.00	19.00	16.00	15.00	20.00	12.00	14.00	12.00	13.00
Measured soil volumetric water content by gravimetric method (%)	6.00	9.10	16.00	13.60	16.40	2.00	6.00	4.70	11.00	10.00	10.70	19.10	18.50	15.10	19.20	11.10	12.50	14.50	11.80
Inversion-measured (%)	-2.00	0.90	3.00	2.40	0.60	0.00	1.00	0.30	2.00	3.00	2.30	-0.10	-2.50	-0.10	0.80	0.90	1.50	-2.50	1.20
Deviation rate (%)	25.00	13.00	17.00	17.00	6.00	12.00	23.00	3.00	20.00	27.00	22.00	3.00	11.00	2.00	5.00	5.00	16.00	20.00	10.00
Calibration depth (cm)	14.0	12.0	26.0	38.0	15.0	12.0	27.0	11.0	13.0	12.0	25.0	15.0	41.0	20.0	40.0	18.0	10.0	28.0	17.0
Wave speed (m/ns)	0.09	0.10	0.10	0.10	0.09	0.07	0.08	0.08	0.09	0.09	0.09	0.10	0.09	0.10	0.10	0.10	0.10	0.10	0.10
Inversion of soil volumetric water content by Topp's model (%)	21.00	17.00	18.00	18.00	23.00	32.00	26.00	26.00	21.00	20.00	21.00	18.00	19.00	16.00	18.00	17.00	17.00	17.00	19.00
Measured soil volumetric water content by gravimetric method (%)	18.10	19.70	18.60	21.30	23.50	26.80	24.70	29.10	18.10	16.30	17.30	16.00	18.10	14.20	21.00	15.50	14.90	15.10	17.90
Inversion-measured (%)	2.90	-2.70	-0.60	-3.30	-0.50	5.20	1.30	-3.10	2.90	3.70	3.70	2.00	0.90	1.80	-3.00	1.50	2.10	1.90	1.10
Deviation rate (%)	14.00	15.00	2.00	17.00	3.00	18.00	6.00	10.00	17.00	24.00	20.00	15.00	4.00	11.00	16.00	7.00	12.00	12.00	4.00
Calibration depth (cm)	25.0	17.0	27.0	15.0	11.0	26.0	10.0	14.0	24.0	16.0	40.0	13.0	9.0	22.0	26.0	10.0	27.0	15.0	11.0
Wave speed (m/ns)	0.10	0.09	0.09	0.08	0.08	0.08	0.10	0.08	0.09	0.09	0.09	0.10	0.09	0.09	0.10	0.09	0.09	0.10	0.10

Table 5 (continued)

Calibration depth (cm)	19.0	19.0	13.0	13.0	20.0	20.0	30.0	17.0	30.0	20.0	13.0	13.0	51.0	26.0	26.0	22.0	25.0	25.0	43.0	20.0	16.0	19.0	19.0	29.0	20.0	49.0
Inversion of soil volumetric water content by Topp's model (%)	16.00	20.00	26.00	26.00	21.00	23.00	19.00	19.00	23.00	19.80	19.00	22.80	21.50	26.00	26.00	19.00	19.00	19.00	19.70	17.00	17.00	17.00	17.00	19.00	20.00	19.00
Measured soil volumetric water content by gravimetric method (%)	17.00	19.70	23.20	23.20	20.70	19.10	20.70	20.70	19.10	19.80	22.80	22.30	21.50	23.20	23.20	20.70	20.70	20.70	19.70	17.00	17.00	17.00	17.00	20.20	16.40	17.20
Inversion-measured (%)	-1.00	0.30	2.80	2.80	-1.70	3.90	-1.70	-1.70	3.90	1.20	-3.80	-2.30	4.50	1.60	1.60	3.00	3.00	3.00	0.30	-1.00	-1.00	-1.00	-1.00	-2.70	-0.40	1.80
Deviation rate (%)	6.00	1.00	12.00	12.00	10.00	23.00	10.00	20.00	23.00	8.00	17.00	9.00	20.00	6.00	6.00	15.00	15.00	15.00	1.00	6.00	6.00	6.00	6.00	13.00	0.00	8.00

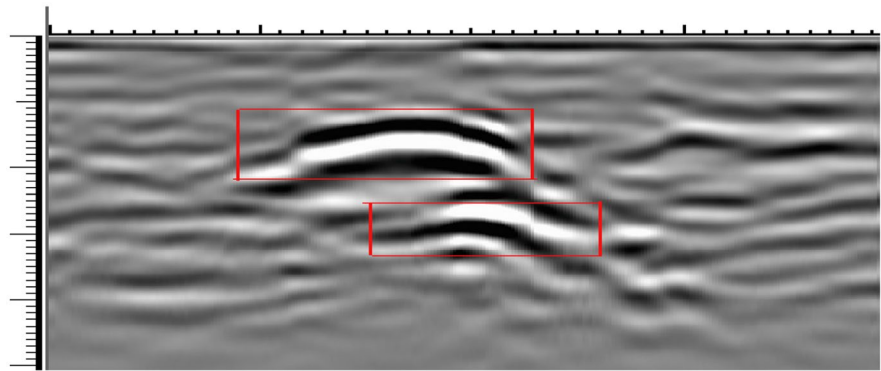
(Yamase et al., 2018; Yu et al., 2018). Similarly, this paper demonstrated that soil gravel content could be detected using GPR. This technology could be used by the reclaimed soil quality supervision department in a mining area to analyze the gravel content of the surface soil.

There were limitations to this study of surface soil gravel content. Isolated gravel with a diameter of less than 1 cm was not detected from a depth of 10–20 cm, and isolated gravel with a diameter less than 2 cm in the depth of 20–30 cm could not be detected, based on the resolution of the aerial. This had an influence on the accuracy of surface soil gravel content results, but this could be addressed by increasing the length of the line to improve the detection accuracy.

Reconstructing soil effective thickness

The GPR could be used to detect the effective soil thickness of the reclaimed land in the mining area. Based on the known electromagnetic wave velocity, relative permittivity, or the soil volumetric water content, the correlation between the calibration depth and the depth of the target in the GPR images was segmented, and the correlation was higher. GPR could be used to accurately determine the effective soil thickness of reclaimed land in mining area. The propagation speed of electromagnetic waves varied across different media over a given time period (Wang et al., 2014). Therefore, the thickness of the soil layer represented on the GPR images was not the true soil thickness. The soil volumetric water content was the main reason affecting the relative permittivity of the medium (Liu et al., 2017). The greater the soil volumetric water content, the larger the relative permittivity, which also affected the propagation velocity of electromagnetic waves in the soil. Therefore, in terms of research methods, the segmentation fitting relationship between the calibration depth and the thickness of the soil layer in the images could be established according to the propagation velocity of the electromagnetic wave in the medium or the relative permittivity of the medium or the relative volume of the soil volumetric water content. This could be used to more accurately quantify the effective soil thickness of the reclaimed land in the mining area. Han et al. (2016) and Hu et al. (2005a,b) used GPR to detect soil stratification; they believed that GPR could be used to

Fig. 10 Evidence of electrical differential media in GPR images



effectively detect stratification in soil, but did not give a method to accurately determine the depth of stratification. Roth et al. (2004) showed that GPR could be used for qualitative exploration of soil layers and shallow groundwater surfaces. Seyfried and Schoebel (2016) used GPR to determine the optimal height for cutting soil. These studies showed that the GPR could be used to determine the effective soil thickness of the reclaimed land in the mining area. In civil engineering, the GPR detection method was based on the type of medium, estimating a relative permittivity based on experience, inputting the GPR main frame, and taking the depth of target (calibrator) represented by GPR images as the true burial depth of target. In the soil, due to the complexity of the underground medium, the soil volumetric water content of the soil was variable. This method of determining the effective soil layer thickness of reclaimed land in the mining area based on experience was prone to error.

This study was able to quantitatively determine the thickness of the soil layer that could inform the process of reclamation of the damaged land in the mining area firstly. Secondly, the thickness of the soil layer could be used to analyze the vegetation status of the reclaimed land.

There were still some deficiencies in this study. Under the influence of detection conditions, when studying the fitting relationship between calibration depth and GPR images depth, the electromagnetic wave velocity ranged from 0.70 to 0.12 ns/m, the soil volumetric water content ranged from 11 to 32%, and the relative permittivity ranged from 6 to 18. Further study is thus required in this regard.

Soil volumetric water content of reclaimed soil

GPR could be used to detect the soil volumetric water content, and the existing Topp’s model was suitable

Table 6 Comparison of soil volumetric water content between measured values and GPR inversion at different depths of sections

Calibration depth (cm)	Wave speed (m/ns)	Relative permittivity	Measured soil volumetric water content (%)	Soil volumetric water content obtained by wave velocity inversion (%)	Measured-inversion (%)	Deviation rate (%)
37	0.0779	14.83	29.20	25.25	3.95	15.6
11	0.0952	9.92	20.04	18.42	1.62	8.8
14	0.0883	11.54	24.61	21.00	3.61	17.2
25	0.0912	10.81	22.09	19.89	2.20	11.1
13	0.0884	11.51	18.05	20.96	-2.91	13.9
11	0.0840	12.76	21.97	22.72	-0.75	3.3
24	0.0863	12.08	19.79	21.78	-1.99	9.1
14	0.0930	10.40	22.57	19.23	3.34	17.4
12.5	0.0742	16.35	29.31	26.86	2.45	9.1
37	0.0831	13.04	26.46	23.09	3.37	14.6

for the calculation of soil volumetric water content in reclaimed land. Shamir et al. used 800-MHz GPR to detect the soil volumetric water content of different types of soil in the laboratory. Compared with the measured soil volumetric water content, the average accuracy was 1.50%. The empirical formula proposed by Topp was the currently accepted industry model for retrieving the soil volumetric water content of sandy soils (Topp et al., 1980). Although the reclaimed land in the mining area was not naturally deposited, the soil could also be investigated by the Topp's model. Wu et al. (2017) used the GPR to detect the soil volumetric water content of reclaimed land in the Shendong mining area in western China. The soil volumetric water content calculated by Topp's model was similar to the measured soil volumetric water content (Wu et al., 2017). In this study, by detecting the soil volumetric water content of the reclaimed land in the mining area, the optimal time to water could be determined during the reclamation process of damaged land in the mining area, thereby promoting vegetation growth and accelerating the vegetation restoration process.

This study was focused on reclaimed land in the coal mining area; the soil volumetric water content was not the only factor affecting the relative permittivity of the soil medium. Further studies are required to determine the suitability of the Topp's model in metal mining area, and to improve the detection accuracy.

Conclusions

In this study, GPR technology was used to detect soil physical properties, such as gravel content, soil volumetric water content, and effective soil layer thickness in a reclaimed coal mine area. The detection results showed that the gravel content of the surface soil could be qualitatively analyzed by the number of isolated gravel signals in the GPR images. As the number of isolated gravel signals was greater, the surface soil gravel content was higher. According to the known relative permittivity or electromagnetic wave velocity or soil volumetric water content, the fitting relationship between the calibration depth and the depth of the calibration of the GPR images was segmented, and the correlation between the two was higher. The fitting relationship R^2 of each segment was higher than 0.940, and the

average value of the five-segment fitting relationship R^2 was 0.966, which indicated that GPR could accurately detect the effective soil thickness of the reclaimed soil in the mining area. GPR could be used to detect the soil volumetric water content of reclaimed land in the mining area, and the Topp's model could be used to calculate soil volumetric water content in reclaimed land in coal mining area.

Our results show that (1) GPR can detect the thickness of soil layer and gravel content of surface soil more quickly and accurately and (2) the Topp model can be used to calculate the volume water content of soil in mining area.

Our research results contribute to the high quality and high efficiency of land consolidation. Using ground penetrating radar to detect soil volume water content in reclamation area can determine the best watering time in the process of vegetation reconstruction, promote vegetation growth, and accelerate vegetation restoration. Using ground penetrating radar to detect the thickness of soil layer in reclamation area can guide to determine the thickness of vegetation in reclamation area and provide basis for researchers to analyze the growth of vegetation in reclamation area. Through the analysis of the surface soil heterogeneity in the reclamation area, the soil quality detection technology is provided for the soil quality management department in the reclamation area.

Funding This work was supported by the National Natural Science Foundation of China (U1810107, 41701607) and the Project for Basic Scientific Research of the Central Universities (2-9-2018-025 and 2-9-2019-307).

Data availability The authors confirm that the data supporting the findings of this study are available within the article.

References

- Anchuela, O. P., Luzon, A., Perez, A. (2016). Ground penetrating radar evaluation of the internal structure of fluvial tufa deposits (Devanos-Anavieja system, NE Spain): an approach to different scales of heterogeneity. *Geophysical Journal International*, ggw167.
- Benedetto, A. (2010). Water content evaluation in unsaturated soil using gpr signal analysis in the frequency domain. *Journal of Applied Geophysics*, 71(1), 26–35.
- Berton, F., Guedes, C. C., Vesely, F. F., De Souza, M. C., Angulo, R. J., Rosa, M. L., & Barboza, E. G. (2019). Quaternary coastal plains as reservoir analogs:

- wave-dominated sand-body heterogeneity from outcrop and ground-penetrating radar, central Santos Basin, southeast Brazil. *Sedimentary Geology*, 97–113.
- Cao, Y., Bai, Z., Sun, Q., & Zhou, W. (2017). Rural settlement changes in compound land use area: characteristics and reasons of changes in a mixed mining-rural-settlement area in shanxi province, china. *Habitat International*, 61, 9–21.
- Cao, Y., Dallimer, M., Stringer, L. C., Bai, Z., & Siu, Y. L. (2018). Land expropriation compensation among multiple stakeholders in a mining area: explaining “skeleton house” compensation. *Land Use Policy*, 74, 97–110.
- Carl PE., & Peter H. (1996). Estimating stone and boulder content in forest soils-evaluating the potential of surface penetration methods. *Catena*, 28(2), 121–134.
- Cerda A. (2001). Effects of rock fragment cover on soil infiltration, interrill runoff and erosion. *European Journal of Soil Science*, 52(1):59–68.
- Certini, G., Campbell, C. D., & Edwards, A. C. (2004). Rock fragments in soil support a different microbial community from the fine earth. *Soil Biology & Biochemistry*, 36(7), 1119–1128.
- Chen, X. Y., Wang, F., Yan, J. P., Liu, Y., Tan, H. Y., & Zhou, Y. Z. (2016). Effects of covering soil thickness on diurnal variation of respiratory soil respiration in mining area. *Journal of China University of Mining & Technology*, 45(1), 163–169.
- Ersahin, S., & Brohi, A. R. (2006). Spatial variation of soil water content in topsoil and subsoil of a typic ustifluvent. *Agricultural Water Management*, 83(1–2), 0–86.
- Guo, J. Y., He, J. L., Li, J. R., Xing, E. D., & Liang, Z. Q. (2015). Effects of artificial remolded landforms on soil erosion in Xilin Gol grassland and its control effects. *Journal of Soil and Water Conservation*, 29(1), 56–61.
- Guo, X. Y., Zhang, J. T., Gong, H. L., & Dong, Z. (2005). Diversity of vegetation restoration process in reclaimed land in Antaibao mining area. *Chinese Journal of Ecology*, 22(4), 763–770.
- Han, X. L., Liu, J. T., Zhang, J., & Zhang, Z. C. (2016). Identifying soil structure along headwater hillslopes using ground penetrating radar based technique. *Journal of Mountain Science*, 13(3), 405–415.
- He, R. Z., Hu, Z. Q., Wang, J., & Wang, Ping. (2009). The progress of using ground penetrating radar to detect the soil quality. *Progress in Geophysics*, 24(4), 1483–1492.
- Hu, Z. Q., Chen, B. Z., & Chen, X. Y. (2005a). Application of ground penetrating radar to detect layered structure of reclaimed soil. *China Mining Industry*, 14(3), 73–75.
- Hu, Z. Q., Wei, Z. Y., & Qin, P. (2005). Concept and method of soil reconstruction in mine reclamation. *Journal of Soils*, 37(1), 8–12.
- Huang, Y. Z., Zhu, Y. G., Tong, Y. P., Hu, Y., & Liu, Y. X. (2004). Effects of soil moisture on the uptake and accumulation of cadmium in maize seedlings. *Chinese Journal of Ecology*, 24(12), 2832–2836.
- Hubbard, S. S., Grote, K. R., & Rubin, Y. (2002). Mapping the volumetric soil water content of a California vineyard using high-frequency GPR ground wave data. *Geophysics*, 21(6), 552–559.
- Lei, S. G., & Bian, Z. F. (2008). Review of the research on determination of soil volume and moisture content by ground penetrating radar. *Chinese Journal of Soil Science*, 39(5), 1179–1183.
- Li, S. (2018). Coal: 22 work points in 2018, capacity announcement 4.36 billion tons. *Energy*, (5): 16.
- Li, X. J., Hu, Z. Q., Jing, L., Ning, L., & Zhang, W. (2007). Research progress of reclaimed soil quality in mining subsidence area. *Transactions of the Chinese Society of Agricultural Engineering*, 23(6), 276–280.
- Li, Y., Shang, S. Y., & Liu, Z. X. (2016). Correlation between the coverage of typical steppe vegetation and the spatial heterogeneity of chestnut soil thickness in Deligor. *Jiangsu Agricultural Sciences*, 44(11), 41–418.
- Liang, F. H. (2012). Preliminary study on detection technology of ground penetrating radar. *Journal of Transportation Research*, 2, 63–66.
- Liu, S. K., Zhao, G. Z., Li, Z. P., Zhou, X., & An, J. (2017). Study on the influence of chromium (Cr) pollution on soil dielectric properties. *Engineering Investigation*, 45(4), 68–74.
- Ma, X. Q., Bi, H. L., Sun, Y., & Zu, H. J. (2012). Environmental geological problems and prevention and control suggestions for mines in Qinghai Province. *Qinghai Environment*, 3, 135–137.
- Meerveld, T. V., & McDonnell, J. J. (2006). On the interrelations between topography, soil depth, soil moisture, transpiration rates and species distribution at the hillslope scale. *Advances in Water Resources*, 29(2), 293–310.
- Ministry of Land and Resources of PRC. TD/T 1036—2013 Completion standards on land reclamation quality. Beijing: China Standards Press, 2013.
- Neal, A. (2004). Ground-penetrating radar and its use in sedimentology: principles, problems and progress. *Earth Science Reviews*, 66(3–4), 261–330.
- Qian, R. Y., Wang, Z. C., Kong, X. C., & Ji, Y. P. (2004). Application of ground penetrating radar to non-metal pipeline detection. *Municipal Technology*, 22(5), 327–329.
- Ratto, C. R., Morton, K. D., Collins, L. M., & Torriero, P. A. (2014). Analysis of linear prediction for soil characterization in gpr data for countermining applications. *Sensing and Imaging*, 15(1), 86–440.
- Roth, K., Wollschlager, U., Cheng, Z. H., & Zhang, J. B. (2004). Exploring soil layers and water tables with ground-penetrating radar. *Pedosphere*, 14(3), 273–282.
- Seyfried, D., & Schoebel, J. (2016). Ground penetrating radar for asparagus detection. *Journal of Applied Geophysics*, 126, 191–197.
- Shakas, A., & Linde, N. (2017). Apparent apertures from ground penetrating radar data and their relation to heterogeneous aperture fields. *Geophysical Journal International*, 3, 1418–1430.
- Topp, G. C., Davis, J. L., & Annan, A. P. (1980). Electromagnetic determination of soil water content: measurements in coaxial transmission lines. *Water Resources Research*, 16(3), 574–582.
- Wang, H. L., Zhang, X., & Sheng, W. Y. (2014). Design and experiment of shrub moisture sensor based on TDT principle. *Transactions of the Chinese Society of Agricultural Machinery*, 5, 259–264.
- Wang, L. B. (2011). The State Council promulgated the implementation of the Land Reclamation Regulations, and the Land Reclamation Regulations promulgated on

- November 8, 1988 were simultaneously abolished. Land and Resources News, (5): 6–9+1.
- Wang, Q. F., Zhou, K. F., Sun, L., Qin, Y. F., & Li, G. Y. (2013). Experimental study on rapid determination of soil water content based on ground penetrating radar[J]. *Journal of Natural Resources*, 28(5), 881–888.
- Wang, X. Y., Li, C. X., Xu, Q. X., & Cai, C. F. (2011). Research progress of gravel covering on soil water erosion process. *China Journal of Soil and Water Conservation*, 9(1), 115–120.
- Wang, Z. C., & Wu, Y. (2010). Geological radar technology for nondestructive testing of tunnel quality. *Railway Technology Innovation*, 3, 78–80.
- Wu, Y. B., Cui, F., Wang, L., Chen, J., & Li, Y. Y. (2014). Detection of soil moisture content by transmissive ground penetrating radar. *Transactions of the Chinese Society of Agricultural Engineering*, 30(17), 125–131.
- Wu, Z. Y., Yin, S. X., & Ma, L. H. (2017). Research on the change of surface soil volume and moisture content in coal mining area based on ground penetrating radar. *Journal of North China Institute of Science and Technology*, 14(6), 17–23.
- Yamase, K., Tanikawa, T., Dannoura, M., Ohashi, M., Todo, C., Ikeno, H., Aono, K., & Hirano, Y. (2018). Ground-penetrating radar estimates of tree root diameter and distribution under field conditions. *Trees-Structure and Function*, 32(6), 1657–1668.
- Yang, F., Du, C., Liang, Y. C., & Xu, X. J. (2014). Exploration of metal mining area based on ground-penetrating radar wave velocity tomography. *Progress in Geophysics*, 29(3), 1332–1336.
- Ye, B. Y., Bai, Z. K., Kong, D. K., & Yu, Y. N. (2008). Remote sensing survey of land destruction and land reclamation dynamic changes in Antaibao Open-Pit Coal Mine. *Journal of University of Science and Technology Beijing*, 30(9), 972–976.
- Yu, B., Che, S., & Cai, S. (2018). Constructing root-seepage-promoting garden plant community comprises e.g. determining the root thickness, root density, and root spatial morphology of common garden plants by ground penetrating radar: Chinese, CN108157111-A[P]. 2018–06–15
- Yu, X. X., Ma, X. W., Di, L. X. T., Liu, H., Xu, Y. M., & Li, B. G. (2011). Experimental study of ground penetrating radar in soil thickness investigation. *Journal of Soil Science*, 48(4), 874–878.
- Yu, Y. J., Ren, S. S., Guo, L. K., & Bi, B. (2016). Study on soil water storage characteristics of two types of reconstructed coal mines. *Soil and Water Conservation Research*, 23(2), 44–48.
- Zenone, T., Morelli, G., Teobaldelli, M., Fischanger, F., Matteucci, M., Sordini, M., Armani, A., Ferre, C., Chiti, T., Seufert, G., et al. (2008). Preliminary use of ground-penetrating radar and electrical resistivity tomography to study tree roots in pine forests and poplar plantations. *Functional Plant Biology*, 35(10), 1047.

Publisher's Note Springer Nature remains neutral with regard to jurisdictional claims in published maps and institutional affiliations.